Research Article | Vol. 25, No. 5 | 6 Mar 2017 | OPTICS EXPRESS 4598

Optics EXPRESS

Tuning out disorder-induced localization in nanophotonic cavity arrays

SERGEI SOKOLOV,[1,2,*] JIN LIAN,[1] EMRE YÜCE,[3] SYLVAIN COMBRIÉ,[4] ALFREDO DE ROSSI,[4] AND ALLARD P. MOSK[1,2]

[1]*Nanophotonics, Debye Institute for Nanomaterials Science, Center for Extreme Matter and Emergent Phenomena, Utrecht University, P.O. Box 80.000, 3508 TA Utrecht, The Netherlands*
[2]*Complex Photonic Systems (COPS), MESA+ Institute for Nanotechnology, University of Twente, P.O. Box 217, 7500 AE Enschede, The Netherlands*
[3]*Light & Matter Control Group, Department of Physics, Middle East Technical University, 06800 Ankara, Turkey*
[4]*Thales Research & Technology, Route Départementale 128, 91767 Palaiseau, France*
[*]*s.a.sokolov@uu.nl*

Abstract: Weakly coupled high-Q nanophotonic cavities are building blocks of slow-light waveguides and other nanophotonic devices. Their functionality critically depends on tuning as resonance frequencies should stay within the bandwidth of the device. Unavoidable disorder leads to random frequency shifts which cause localization of the light in single cavities. We present a new method to finely tune individual resonances of light in a system of coupled nanocavities. We use holographic laser-induced heating and address thermal crosstalk between nanocavities using a response matrix approach. As a main result we observe a simultaneous anticrossing of 3 nanophotonic resonances, which were initially split by disorder.

OCIS codes: (350.4238) Nanophotonics and photonic crystals; (260.5740) Resonance; (140.3945) Microcavities; (090.1995) Digital holography.

References and links

1. A. Yariv, Y. Xu, R. K. Lee, and A. Scherer, "Coupled-resonator optical waveguide: a proposal and analysis," Opt. Lett. **24**, 711–713 (1999).
2. P. Hamel, S. Haddadi, F. Raineri, P. Monnieri, G. Beaudoin, I. Sagnes, A. Levenson, and A. M. Ya, "Spontaneous mirror-symmetry breaking in coupled photonic-crystal nanolasers," Nat. Photon. **9**, 311–315 (2015).
3. D. Gerace, H. E. Türeci, A. Imamoglu, V. Giovannetti, and R. Fazio, "The quantum-optical Josephson interferometer," Nature Phys. **5**, 281–284 (2009).
4. E. Parra and J. R. Lowell, "Toward Applications of Slow Light Technology," Opt. Photonics News **18**, 40 (2007).
5. F. Morichetti, C. Ferrari, A. Canciamilla, and A. Melloni, "The first decade of coupled resonator optical waveguides: Bringing slow light to applications," Laser Photon. Rev. **6**, 74–96 (2012).
6. H. Takesue, N. Matsuda, E. Kuramochi, W. J. Munro, and M. Notomi, "An on-chip coupled resonator optical waveguide single-photon buffer." Nat. Commun. **4**, 2725 (2013).
7. E. Kuramochi, K. Nozaki, A. Shinya, K. Takeda, T. Sato, S. Matsuo, H. Taniyama, H. Sumikura, and M. Notomi, "Large-scale integration of wavelength-addressable all-optical memories on a photonic crystal chip," Nat. Photon. **8**, 474–481 (2014).
8. M. Notomi, E. Kuramochi, and T. Tanabe, "Large-scale arrays of ultrahigh-Q coupled nanocavities," Nat. Photon. **2**, 741–747 (2008).
9. K. Fang, M. H. Matheny, X. Luan, and O. Painter, "Optical transduction and routing of microwavephonons in cavity-optomechanical circuits," Nat. Photon. **10**, 489–496 (2016).
10. M. Tillmann, B. Dakić, R. Heilmann, S. Nolte, A. Szameit, and P. Walther, "Experimental boson sampling," Nat. Photon. **7**, 540–544 (2013).
11. M. L. Cooper, G. Gupta, M. a. Schneider, W. M. J. Green, S. Assefa, F. Xia, Y. a. Vlasov, and S. Mookherjea, "Statistics of light transport in 235-ring silicon coupled-resonator optical waveguides," Opt. Express **18**, 26505–26516 (2010).
12. F. Sgrignuoli, G. Mazzamuto, F. Intonti, F. S. Cataliotti, M. Gurioli, and C. Toninelli, "Necklace State Hallmark in Disordered 2D Photonic Systems," ACS Photonics **2**, 1636–1643 (2015).
13. Y. Taguchi, Y. Takahashi, Y. Sato, T. Asano, and S. Noda, "Statistical studies of photonic heterostructure nanocavities with an average Q factor of three million," Opt. Express **19**, 11916–11921 (2011).

#280949 https://doi.org/10.1364/OE.25.004598
Journal © 2017 Received 15 Nov 2016; revised 20 Jan 2017; accepted 21 Jan 2017; published 21 Feb 2017

Optics EXPRESS

14. L. Ramunno and S. Hughes, "Disorder-induced resonance shifts in photonic crystal nanocavities," Phys. Rev. B **79**, 161303 (2009).
15. A. Faraon, D. Englund, D. Bulla, B. Luther-Davies, B. J. Eggleton, N. Stoltz, P. Petroff, and J. Vučković, "Local tuning of photonic crystal cavities using chalcogenide glasses," Appl. Phys. Lett. **92**, 043123 (2008).
16. C. J. Chen, J. Zheng, T. Gu, J. F. McMillan, M. Yu, G.-Q. Lo, D.-L. Kwong, and C. W. Wong, "Selective tuning of high-Q silicon photonic crystal nanocavities via laser-assisted local oxidation." Opt. Express **19**, 12480–12489 (2011).
17. T. Cai, R. Bose, G. S. Solomon, and E. Waks, "Controlled coupling of photonic crystal cavities using photochromic tuning," Appl. Phys. Lett. **102**, 2238 (2013).
18. M. Notomi, A. Shinya, S. Mitsugi, G. Kira, E. Kuramochi, and T. Tanabe, "Optical bistable switching action of Si high-Q photonic-crystal nanocavities," Opt. Express **13**, 2678–2687 (2005).
19. B. A. Ruzicka, L. K. Werake, H. Samassekou, and H. Zhao, "Ambipolar diffusion of photoexcited carriers in bulk GaAs," Appl. Phys. Lett. **97**, 262119 (2010).
20. S. Sokolov, J. Lian, E. Yüce, S. Combrié, G. Lehoucq, A. De Rossi, and A. P. Mosk, "Local thermal resonance control of GaInP photonic crystal membrane cavities using ambient gas cooling," Appl. Phys. Lett. **106**, 171113 (2015).
21. S. Combrié, A. De Rossi, Q. V. Tran, H. Benisty, "GaAs photonic crystal cavity with ultrahigh Q: microwatt nonlinearity at 1.55 micron." Opt. Lett. **33**, 1908–1910 (2008).
22. M. Pasienski and B. DeMarco, "A high-accuracy algorithm for designing arbitrary holographic atom traps." Opt. Express **16**, 2176–2190 (2008).
23. J. Lian, S. Sokolov, E. Yüce, S. Combrié, A. De Rossi, A. P. Mosk, "Measurement of the profiles of disorder-induced localized resonances by local tuning," Opt. Express **24**, 21939–21947 (2016).
24. J. Lian, S. Sokolov, E. Yüce, S. Combrié,A. De Rossi, and A. P. Mosk, "Fano lines in the reflection spectrum of directly coupled systems of waveguides and cavities: measurements, modeling and manipulation of the Fano asymmetry," arXiv: 1610.08351 [physics.optics] (2016).
25. W. Zhou, D. Zhao, Y. C. Shuai, H. Yang, S. Chuwongin, A. Chadha, J. H. Seo, K. X. Wang, V. Liu, Z. Ma, and S. Fan, "Progress in 2D photonic crystal Fano resonance photonics," Prog. Quant. Electron. **38**, 1–74 (2014).
26. H. A. Haus and W. Huang, "Coupled-mode theory," Proc. IEEE **79**, 1505–1518 (1991).
27. J. Joannopoulos, S. G. Johnson, J. N. Winn, and R. D. Meade, *Photonic Crystals: Molding the Flow of Light* (Princeton University Press, Princeton, 2008).
28. R. Lauter, C. Brendel, S. J. M. Habraken, and F. Marquardt, "Pattern phase diagram for two-dimensional arrays of coupled limit-cycle oscillators," Phys. Rev. E **92**, 012902 (2015).
29. K. Nozaki, E. Kuramochi, A. Shinya, and M. Notomi, "25-channel all-optical gate switches realized by integrating silicon photonic crystal nanocavities," Opt. Express **22**, 3491–3496 (2014).
30. A. C. Liapis, B. Gao, M. R. Siddiqui, Z. Shi, and R. W. Boyd, "On-chip spectroscopy with thermally-tuned high-Q photonic crystal cavities," Appl. Phys. Lett. **108**, 021105 (2016).
31. X. Gan, N. Pervez, I. Kymissis, F. Hatami, and D. Englund, "A high-resolution spectrometer based on a compact planar two dimensional photonic crystal cavity array," Appl. Phys. Lett. **100**, 4177 (2012).
32. S. Mittal, J. Fan, S. Faez, A. Migdall, J. M. Taylor, and M. Hafezi, "Topologically robust transport of photons in a synthetic gauge field," Phys. Rev. Lett. **113**, 087403 (2014).
33. J. Bertolotti, S. Gottardo, D. S. Wiersma, M. Ghulinyan, and L. Pavesi, "Optical necklace states in anderson localized 1D systems," Phys. Rev. Lett. **94**, 1–4 (2005).
34. J. B. Spring, B. J. Metcalf, P. C. Humphreys, W. S. Kolthammer, X.-M. Jin, M. Barbieri, A. Datta, N. Thomas-Peter, N. K. Langford, D. Kundys, J. C. Gates, B. J. Smith, P. G. R. Smith, and I. A. Walmsley, "Boson Sampling on a Photonic Chip," Science **339**, 798–801 (2013).
35. A. Crespi, R. Osellame, R. Ramponi, D. J. Brod, E. F. Galvão, N. Spagnolo, C. Vitelli, E. Maiorino, P. Mataloni, and F. Sciarrino, "Integrated multimode interferometers with arbitrary designs for photonic boson sampling," Nat. Photon. **7**, 545–549 (2013).

1. Introduction

Optical circuits containing high-Q photonic crystal nanocavities have been proposed for delay lines, optical memory storage, optomechanics and quantum communication [1–10]. However, unavoidable fabrication disorder in nanophotonic structures causes scattering which leads to frequency detuning, signal attenuation, and eventually localizes optical modes which ruins the transmission properties of the whole system [11, 12]. Even state-of-the-art nanofabrication with random spatial variations of only $\Delta x = 1$ nm can lead to resonance wavelength detunings of more than $\Delta\lambda = 1$ nm [13, 14].

Several methods have been proposed to tune nanocavities. Methods based on local refractive index change, such as photodarkening, photoactivation and photo-oxidation [15–17], have limited

Optics EXPRESS

tuning range and irreversibility as well as introduction of optical loss. Other methods which involve free-carriers or heat suffer from diffusion, namely free-carriers and heat diffuse far beyond the physical size of the cavity [18–20]. Since in a system with a useful optical coupling between nanocavities elements should be placed physically close to each other, this results in unavoidable crosstalk in the tuning process. In addition, in high-Q systems carriers dissipate on a time scale comparable to or shorter than the resonance lifetime.

In this paper, we demonstrate a new approach for realignment of resonances of closely-spaced cavities based on holographic thermal tuning. By accurately measuring the thermal response of resonance wavelength in the system and obtaining the power settings required to hybridize cavities, we experimentally align an array of three nanocavities, which were initially misaligned by more than 200 unloaded resonator linewidths. Our method is scalable to large arrays and enables programmable photonic devices where circuit functionalities can be dynamically switched on and off.

2. Sample and experimental setup

The sample under investigation is $Ga_{0.51}In_{0.49}P$ air-suspended photonic crystal membrane with thickness $d = 180$nm. Three nanocavities are defined in a photonic crystal waveguide with width of $0.98\sqrt{3}a$ made in a hexagonal lattice with period $a = 485$ nm and hole radius $r = 0.28a$. They are defined by local width modulation [21] of the waveguide with a maximum hole shift of $0.0124a$. An out-of-line waveguide with a width $1.1\sqrt{3}a$ is used to couple light in and out of the system. The distance between cavity 1 and cavity 2 is 4.4 μm, and the distance between cavity 2 and 3 is 4.9 μm. Numerically calculated coupling rates are $\Gamma_{12} = 0.00022\omega_0$ and $\Gamma_{23} = 0.00015\omega_0$, where ω_0 is the resonance wavelength of the cavity, Γ_{jk} is a coupling rate between cavity j and k.

The setup for the thermal control is shown in Fig. 1(a). CW pump light ($\lambda = 405$ nm) is used to thermally tune nanocavities. A reflective liquid crystal spatial light phase modulator (SLM) was imaged onto the back aperture of the objective to holographically [22] create several focused spots on the sample. Light was focused into tight spots with FWHM 0.8 μm. The absolute intensity of all pump spots was measured using a CCD camera placed in the reflection configuration and calibrated with a power meter. To attribute a particular resonance to a particular cavity we performed pump line-scans of the pump spot along the cavity array [20, 23]. The resulting linescan of our sample is presented in Fig. 2. The closer the pump spot to the center of a particular cavity the bigger the overlap of the temperature profile created by the pump laser and mode profile of the cavity. This allows to easily identify resonances, as indicated in Fig. 2. The resonances of cavities 1 and 2 are easily visible in the graph. Resonance 3 is shallow and narrow (See Fig.2(b)), and while it is measured with signal-to-noise ratio >5 it is not obvious on the printed graph. So its position is indicated by black markers. In addition to resonance lines there are also wide fringes present in Fig. 2. These fringes results from interference in the system and are addressed in detail in Ref. 24. To extract resonance wavelengths and widths the reflection spectra were fitted with appropriate Fano line-shape of the resonances [25], as it is shown in Fig. 1(b).

3. Thermal response matrix approach

When a photonic crystal membrane is heated with focused CW laser light the width of the temperature profile is more than 4 times larger than the diffraction-limited laser focus [16, 20]. Although this width can be tailored by properly selecting the material of the membrane and the ambient media [20], significant crosstalk remains for any choice of material. To account for that crosstalk we employ a response matrix approach. In the linear tuning regime, where the resonance shift is proportional to the applied power, we construct a matrix (M_{ij}) which expresses

Optics EXPRESS

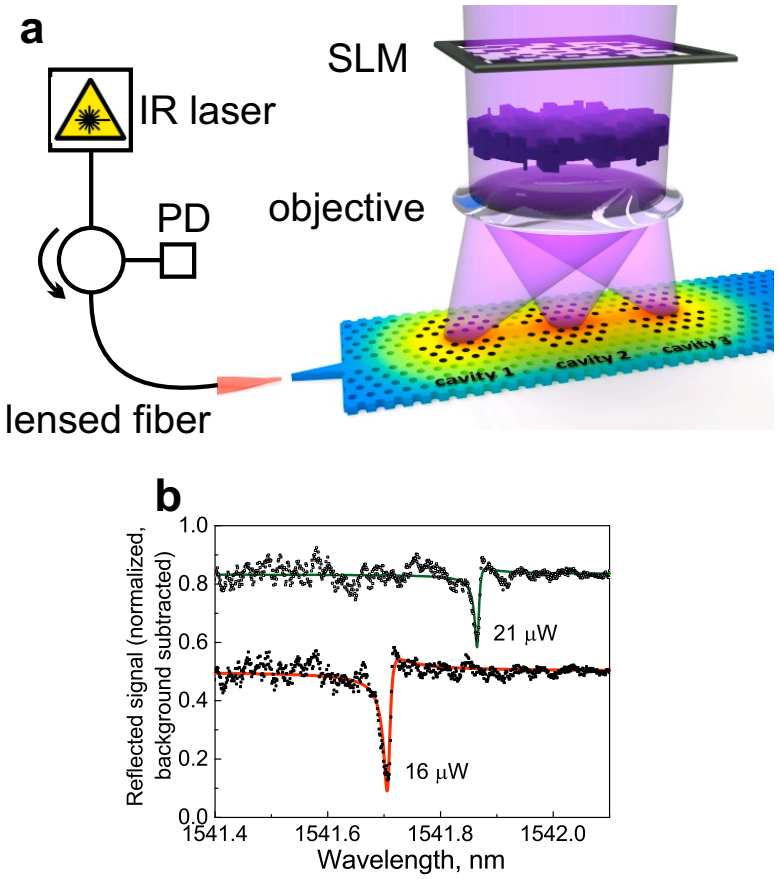

Fig. 1. **Schematic of the experiment. a** Pump light is modulated by the SLM to holographycally create several focused spots on the sample. The SLM is imaged to the pupil of the objective. Continuous wave IR probe light from a tunable laser with TE polarization is coupled to the sample through a polarization maintaining lensed fiber and the reflected signal is collected on a photodiode using a fiber circulator. **b** Reflection spectra showing the resonance of cavity 3 for pump powers 16 μW and 21 μW. Power applied to cavity 1 is 9 μW. Solid lines represent Fano fits. The smoothed background is subtracted, offset is applied for clarity.

the response of the resonance wavelength ($\Delta\lambda_i$) to the applied pump powers P_i:

$$\Delta\lambda_i = \sum_j M_{ij} \cdot P_j \tag{1}$$

Diagonal elements of the response matrix determine the response of the addressed cavity and off-diagonal elements determine crosstalk to the neighbors. Ideally the response matrix values can be calculated [20], however they are sensitive to experimental details, therefore we use measured values.

We place a single pump spot on top of each cavity at a time and measure resonance redshift versus applied pump power. The result is presented in Figs. 3(a,b,c) for cavity 1, 2 and 3 respectively. In some cases when cavity resonances occur too close together, a second pump spot is placed to bias the resonance, as in Fig. 3(c). Resonance shifts are then fitted with linear dependencies, where slopes give thermal crosstalk values. The cavity directly under the pump

Optics EXPRESS

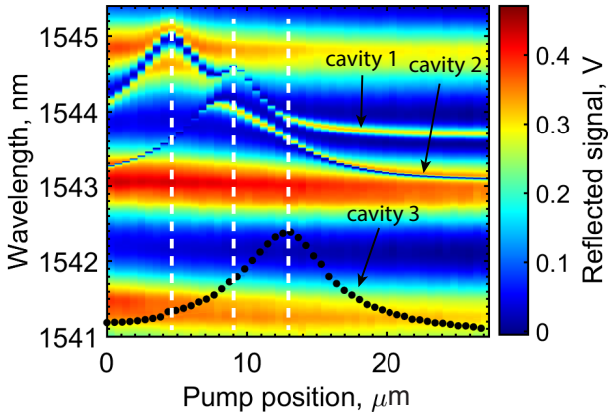

Fig. 2. **Pump line-scan.** Response of cavity resonances for pump placed at different positions. The power on the surface of the sample is 32 μW. Black dots indicate resonance of the cavity 3 for better visibility. White dashed lines indicate cavity positions.

spot displays the steepest slope whereas resonances of neighbor cavities have smaller slopes. The measured response matrix is

$$M = \begin{pmatrix} 4.1 & 1.6 & 0.6 \\ 1.6 & 3.6 & 1.5 \\ 0.7 & 1.6 & 3.3 \end{pmatrix} \cdot 10^{-2} \frac{\text{nm}}{\mu\text{W}} \tag{2}$$

Response values differ slightly from cavity to cavity as a consequence of positioning accuracy of pump spots, the difference in physical separation between cavities and possible differences in local surface reflectivity and thermal conductivity. On average first-neighbor crosstalk is 44%, whereas second-neighbor crosstalk is 17%. Such levels of thermal crosstalk cannot be neglected. We find bare wavelengths of nanocavity resonances to be 1543.78 ± 0.11 nm for cavity 1, 1543.02 ± 0.04 nm for cavity 2 and 1541.1 ± 0.04 nm for cavity 3, which matches with reference measurements. Due to the disorder cavity 3 is detuned from cavities 1 and 2 by about $\Delta\lambda = 2$ nm. The observed detunings can be explained by disorder, taking into account our fabrication accuracy of $\Delta x \approx 4$ nm.

4. Alignment of the array

To find the required powers and the target wavelength at which all the resonances anticross we solve the resulting linear programming problem. The condition for this problem is that all applied powers are positive. We find that the target wavelength is 1544.79 nm and corresponding powers are $P_1 = 9$ μW, $P_2 = 0$ μW and $P_3 = 108$ μW. As a result of the procedure the lowest applied pump power is always zero, therefore to align three resonances 2 pump spots are sufficient. In general to align N cavities one needs to place at least $N - 1$ pump spots on the surface of the sample, as in Eq. 1 we have N equations but $N + 1$ variables, therefore there is a freedom to select the power of one of the pump spots to be 0.

In Fig. 4(a) we show the hybridization of the three resonances which is the main result of this paper. We set P_1 to the calculated value and gradually increase P_3 and plot resonance wavelengths. The resonances anticross and become fully hybridized at around 108 μW. The reflection spectra for this power is shown in Fig. 4(c). In the region where resonances are hybridized they cannot be attributed to a particular cavity, hence we label them as resonance I, II and III. At low pump powers resonances I, II and III represent cavities 1,2 and 3 correspondingly. At high powers after the resonances anticross, resonance I localizes on cavity 3 and resonance III localizes on cavity

Optics EXPRESS

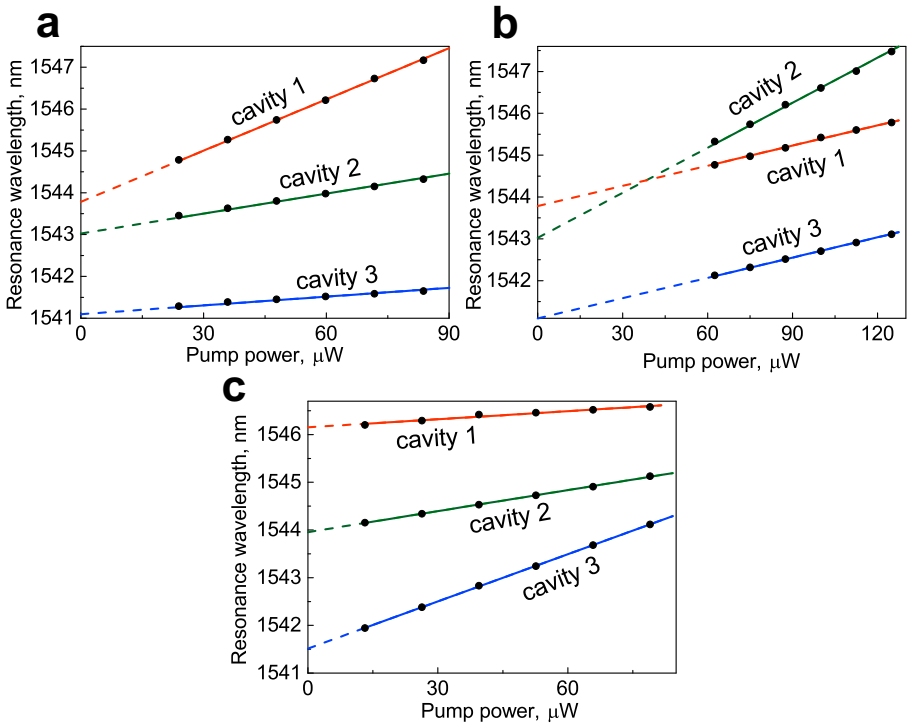

Fig. 3. **Determination of the thermal response matrix. a**,**b**,**c** Response curves of cavity resonances to pump spots placed on top of cavity 1 (**a**),2 (**b**),3 (**c**). Solid lines are line fits to experimental data and dashed lines are extrapolation of fitting curves to the zero power. In **c** cavity 1 was biased with 60 μW pump power to separate the resonances.

1. For pump powers higher than 140 μW, resonance I becomes very weak and its wavelength cannot be extracted.

In case of weak optical coupling between cavities the behavior of the resonances can be described by coupled-mode theory [26] assuming only nearest-neighbor coupling. The result is presented in Fig. 4(a). To find coupling rates for our cavities the parameters of the coupled-mode model were adjusted in the region where cavities are coupled, i.e. for powers between 70 and 140 μW. We find good agreement between theory and experiment and obtain coupling rates which are equal to $\Gamma_{12} = (0.90 \pm 0.29) \cdot 10^{-4} \cdot \omega_0$, $\Gamma_{23} = (1.92 \pm 0.27) \cdot 10^{-4} \cdot \omega_0$, or equivalently $\Gamma_{12} = 0.14 \pm 0.05$ nm and $\Gamma_{23} = 0.30 \pm 0.04$ nm.

The experimentally determined values of the coupling rates are different from the numerically calculated ones. This suggests that disorder affects not only the resonance wavelength and Q-factor, but also the mode profile of a cavity, which determines the coupling constant [26].

The widths of all three resonances are expected to change while the cavities anticross. Cavity 1 is the closest cavity to the input waveguide which suggests that it should have the largest width due to the leak to the waveguide. At the same time when cavities are coupled the leakage from second and third cavity to the waveguide should increase, and resonances II and III should broaden. In Fig. 4(b) the experimental dependence of the widths of the resonances on applied power P_3 is presented. The width of the resonance I slowly decreases with pump power P_3 and becomes very narrow at high pump powers confirming that it has become localized on cavity 3. The inverse dependence is pronounced for resonance III which starts localized on cavity 3 and ends on cavity 1. At the point of anticrossing resonance II becomes the broadest. The width

Optics EXPRESS

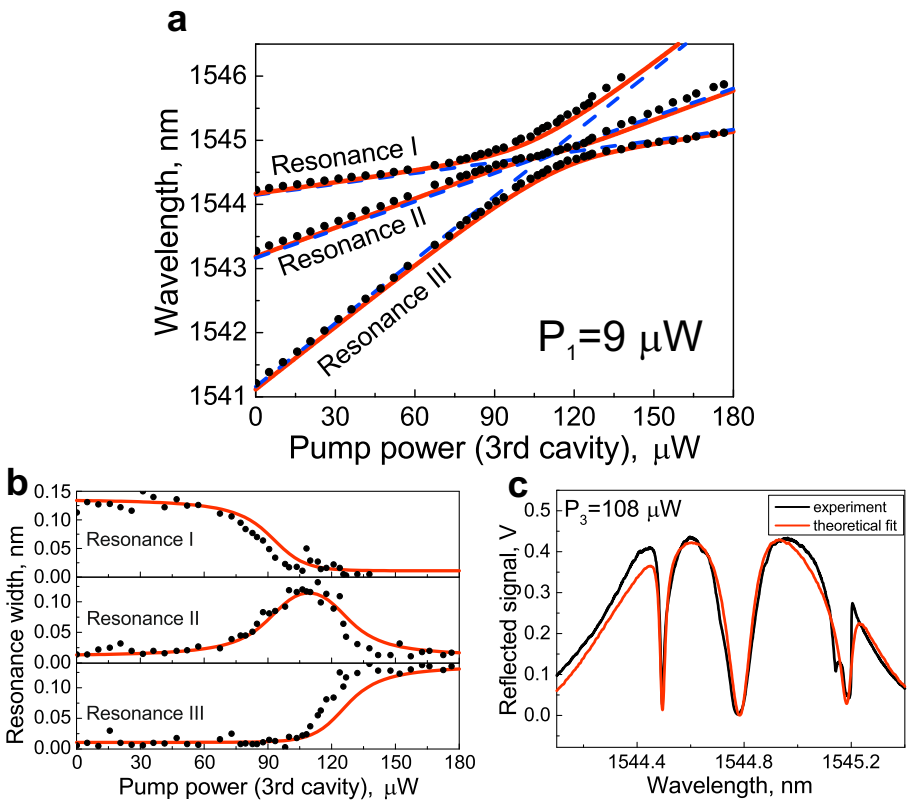

Fig. 4. **Alignment of cavity resonances.** Resonance positions **a** and widths **b** are obtained from reflection spectra by fitting Fano lineshapes. The pump power for cavity 1 was fixed to 9 μW, while the power for cavity 3 was increased from 0 to 180 μW. Red solid line is a fit by coupled-mode theory. Blue dashed lines represent uncoupled resonance wavelengths. **c** - Spectra of the sample for $P_3 = 108\mu$W Red solid line represents Fano line fit with 3 resonance lines and 5th order polynomial as a background.

of the resonances can be predicted using temporal coupled-mode theory [27] where we take into account the influence of the input waveguide and radiation loss. The model is presented in Fig. 5. Cavities 2 and 3 are placed physically away from the input waveguide and therefore the coupling rates between them and the waveguide can be neglected. These resonances are visible in reflection only due to the light which leaks via the cavity 1. Only nearest neighbor coupling is taken into account. This result in the following system of equations:

$$\begin{cases} S_- = -1 + \sqrt{2\gamma}a_1, \\ \frac{da_1}{dt} = -i\omega_1 a_1 - i\Gamma_{12}a_2 - a_1\gamma - a_1\gamma_0 + \sqrt{2\gamma}, \\ \frac{da_2}{dt} = -i\omega_2 a_2 - i\Gamma_{12}a_1 - i\Gamma_{23}a_3 - a_2\gamma_0, \\ \frac{da_3}{dt} = -i\omega_3 a_3 - i\Gamma_{23}a_2 - a_3\gamma_0 \end{cases} \tag{3}$$

Here γ is a coupling rate to he input waveguide, S_- is a complex amplitude of the outgoing waveguide mode, a_1, a_2 and a_3 are complex amplitude of the field inside cavities, ω_1, ω_2 and ω_3 are bare frequencies of nanocavities and γ_0 determines intrinsic cavity decay rate. We define two free parameters which are the loaded Q-factor of the first cavity (Q_L) and the intrinsic Q-factor (Q_0) of cavities assuming that it is the same for all cavities. We fit these free parameters outside the hybridization region, i.e. for power less than 70 μW and more than 140 μW and

Optics EXPRESS

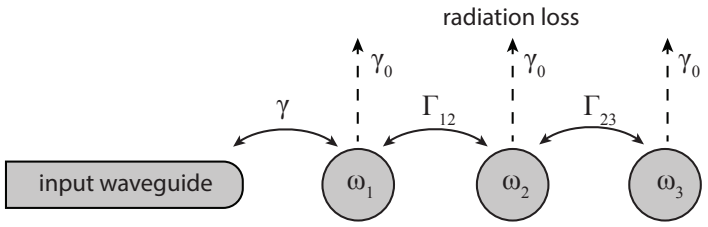

Fig. 5. **Model of the sample.** The light is coupled to the first cavity in the system with coupling rate γ, then each cavity in the array is coupled to the nearest neighbor by coupling constants Γ_{12} and Γ_{23}.

obtain a good agreement with experiment (see Fig. 4(b)). The value for intrinsic Q-factor is found to be $Q_0 = (1.42 \pm 0.45) \cdot 10^5$, while the value of loaded Q-factor for the first cavity is $Q_L = (1.12 \pm 0.05) \cdot 10^4$. The numerically calculated value of the loaded Q-factor is 11000 which matches the value obtained from the experiment.

5. Conclusion

In conclusion, we have proposed and implemented a new method to program individual resonance wavelengths of coupled cavities. We corrected for thermal tuning crosstalk in the system to obtain independent tuning of resonances by measuring the thermal response matrix. We coupled three nanocavities and hybridized their local resonances into spatially extended modes. This shows that our method is capable of counteracting disorder in arrays of coupled cavities. The resonance wavelengths and widths were very well reproduced by a coupled-mode model. Our method can be easily extended to a larger number of nanocavities by adding more pump spots to the system. Resonance tuning with crosstalk compensation is likely to become a valuable method for any type of systems where disorder influences resonance states is required such as optomechanical systems [9,28], many resonator systems [29–32], disordered necklace states [12,33] and complex boson sampling networks [34,35].

6. Methods

The experiment was performed in dry nitrogen atmosphere to minimize oxidation and surface water effects [16]. The sample temperature was locked at 41.85 ± 0.001 °C. To further minimize these effects the illumination time of the surface with pump light was minimized to 270 ms during which the pumped measurement was taken. Nonetheless, minor surface effects were present in the data, resulting in resonance blueshifts and redshifts. To correct for that we performed reference measurement with no pump light immediately after each pumped measurement. Then surface effects for crosstalk matrix coefficients were eliminated by subtracting reference resonance values from pumped ones. As there is significant coupling between resonances 1 and 2 in the unpumped sample, to extract the bare resonance frequencies we used only data taken at pump powers >10 μW. During the final measurement resonance shifts due to above mentioned effects were less than 80 pm for all presented datapoints.

Funding

European Research Council project (ERC) (279248), Nederlandse Organisatie voor Wetenschappelijk Onderzoek (NWO).

Optics EXPRESS

Acknowledgments

The authors would like to thank Sanli Faez, Henri Thyrrestrup and Willem Vos for helpful discussions and advises, Cornelis Harteveld for technical support.